New Algorithm for Three-Dimensional Borehole-to-Surface Apparent Resistivity Imaging Based on Unstructured Mesh Finite-Element Method

ZHITAO XIONG [1,2], **XINGONG TANG** [1,2], **WEIZHONG QIU** [3], **CHUNYAN ZHAO** [4], **AND LIANQUN ZHANG** [5]

[1]Key Laboratory of Exploration Technologies for Oil and Gas Resources of MOE, Yangtze University, Wuhan 430100, China
[2]Hubei Cooperative Innovation Center of Unconventional Oil and Gas, Wuhan 430100, China
[3]Shanxi Coal Geology Exploration Institute, Datong 037039, China
[4]Shanxi 131 Coal Field Geology Limitid Company, Hancheng 715400, China
[5]PetroChina Research Institute of Petroleum Exploration and Development, Beijing 100083, China

Corresponding author: Xingong Tang (18665800697@163.com)

ABSTRACT In this paper, a finite-element method with unstructured mesh is used to numerically simulate the line source model of three-dimensional borehole-to-surface electrical potential method. A new total field potential is synthesized using the calculated anomalous field potential and the analytic solution of the background field. In solving for the original total field potential and background potential, this method can guarantee a small near-field error in the new total field potential without the need to densely mesh the region with the source. By comparing the synthesized total field and analytic solution, the high accuracy of the numerical solution is verified. The results of model calculation show that the detection effectiveness of the borehole-to-surface electrical method depends on the length of the line source. The detection effectiveness increases substantially with increasing length of the line source within a certain range. However, when the line source is excessively long, the increase in detection effectiveness for anomalies is insignificant. For a low-resistance anomaly of a given volume, the borehole-to-surface electrical method is more sensitive to changes in the lateral area than to changes in the thickness. When the gob contains only a small amount of water (e.g., Model IV containing 5% of water by volume), it will appear as a low-resistance anomaly. In addition, the detection of a water-logged gob by the borehole-to-surface electrical method depends on the depth and size of the gob. The borehole-to-surface method can accurately delineate the profile boundary of an anomaly, even though the side closer to the source is susceptible to the effect of source current. These results are significant for guiding the field exploration of the borehole-to-surface electrical method, improving result interpretation, and assisting the application.

INDEX TERMS Borehole-to-surface electrical potential method, finite-element method, vertical line source, unstructured mesh.

I. INTRODUCTION

The borehole-to-surface electric potential method possesses the advantages of both ground surface and borehole electrical prospecting methods. With its advantages of wide detection range, large detection depth, and high resolution, the borehole-to-surface electrical method is widely used in

The associate editor coordinating the review of this manuscript and approving it for publication was Su Yan.

residual oil development and fracturing monitoring, coal mining and detection of water-filled layers, and detection of ores and pollutants [1]–[9]. By injecting the electric current directly into the underground target layer through the borehole, the borehole-to-surface electrical method overcame the difficulty of obtaining high-resolution data due to complex underground structure and deeply buried targets layer encountered by surface prospecting methods [10]. The method also overcomes the difficulty of over-abundant

borehole data but severely insufficient reservoir data in the borehole prospecting method, and can effectively detect the weak signals of deeply buried targets over a wide area. Mine flooding incidents are major disasters in coal mining, with water hazards in mined-out areas accounting for a large proportion of floods [11]. The dire need for mining resources has made it extremely urgent to devise an effective detection method for deeply hidden ores in vulnerable mines [12]. To efficiently determine the distribution of complex concealed orebodies and water-logged gobs underground with the borehole-to-surface electrical method, it is essential that in-depth studies of the borehole-to-surface method be carried out. Such research is highly significant in preventing water hazards and exploiting potential vulnerable mines.

The borehole-to-surface method was first proposed in 1958 by a former Soviet scientist A.M. çaãapìèctp [13]. After extensive investigation and application by numerous researchers, the theory has been substantially developed and there are now abundant application results. Alfano [14] provided an analytical solution of the surface potential of a three-layered dielectric borehole-to-surface model. Pridmore *et al.* [15] carried out a numerical calculation of the three-dimensional (3D) borehole-to-surface potential using the finite-element method. Rocroi and Koulikov [16] injected electric current directly to the target layer through the casing well and discovered two high-abundance zones of by-passed oil in two lithologic traps in an oil-rich region. Scriba [17] and Spitzer [18] simulated the electric potential response of a 3D borehole-to-surface cross-section based on the finite-difference method. Ushijima *et al.* [19] achieved dynamic imaging monitoring of fluid flow in a fracture with the borehole-to-surface potential method. Using a finite-difference technique, Yue and Liu [20] completed the 3D forward calculation in the borehole-to-surface potential method for a point source, and analyzed the structural changes before and after the grouting of a coal mine gob. In water tank simulation experiments, Wang *et al.* [21] studied the response behavior of borehole-to-surface electric potential. In 2006, Xu *et al.* [22] applied finite-difference and conjugate gradient iteration techniques and completed the inversion of the 3D borehole-to-surface resistivity of a vertical line source. Wang *et al.* [23], [24] separately used the Born approximation, quasi-analytical approximation, and weighted regularization conjugate gradient to invert the electromagnetic data of a 3D borehole-to-surface model. Tang *et al.* [25] used the apparent geoelectric resistivity to define the disparity rate, and delineated the reservoir boundary by the disparity rate and its gradient. However, it was difficult to effectively identify the blind mine beside the borehole. Qu *et al.* [26] succeeded in the inversion of 3D borehole-to-surface resistivity using an improved conjugate gradient method and alleviated the ''upward drift'' phenomenon of the electrical anomaly in the inversion. David *et al.* [3] used the target-oriented adaptive finite-element method to simulate the electric field response of the borehole-to-surface electric model. Ho [27] realized rapid inversion of the 3D borehole-to-surface

potential based on neural network technology. Dai *et al.* [28] believed that it was feasible to investigate residual oil distribution with the borehole-to-surface approach based on dual-frequency induced polarization borehole-to-surface electrical experiments conducted at Daqing oil field, China. In 2009, Ke and Huang [29] simulated the potential response of the 3D borehole-to-surface method using the finite-element method. They succeeded in inverting the borehole-to-surface data using the nonlinear damped least-squares method and discussed the effects of noise level and the size of the measurement area on the inversion results. Li *et al.* [10] completed the calculation of the 3D borehole-to-surface potential response with terrain using the finite-element method of unstructured mesh and simulated the anomalous surface potential distribution for different locations of the point source relative to the anomaly. Dai *et al.* [5] used the finite-element technique to calculate the 3D borehole-to-surface potential model for a complex line source. The distribution pattern of line source profoundly affected the distribution of surface potential. Cao *et al.* [30] simulated the electric field response of borehole-to-surface electromagnetic method in the frequency domain with water tank experiments. They experimentally verified the feasibility of delineating the oil and gas target zone using the borehole-to-surface electromagnetic method from an experimental perspective. Wang and Pan [31] conducted numerical simulation of the 3D borehole-to-surface electric potential method for a point source with the finite-element method. The response characteristics of medium-depth and large, deep anomalies were enhanced through the derivative of the total normalized potential, which helped delineate the boundary of the anomaly. Zhang *et al.* [32] calculated the response of 3D borehole-to-surface method using a finite-difference method. Wang *et al.* [33], [34] succeeded in inverting the borehole-to-surface potential model with an inequality-constrained, nonlinear conjugate gradient method and simulated the response features of apparent resistivity and apparent polarization of a line source 2D borehole-to-surface model with terrain using the finite-element method with unstructured mesh.

When electric current is supplied to a stratum through a metal sleeve in the borehole-to-surface electrical method, since the diameter of the sleeve is much smaller than its length, it may be simplified to a line current source of finite length in the forward calculation of the model [35]. Based on this model, we carried out numerical simulation of the line source 3D borehole-to-surface electrical method. The accuracy of the calculation will to some extent be affected by the partition of the mesh of the model and the degree of fitting to the complex boundary. Compared to structured mesh, unstructured mesh can actually handle the irregular multi-scale complex model more effectively. Therefore, we use a finite-element method with unstructured mesh to study the effects of line source length, horizontal and vertical scale change of the model, and the percentage of water in the gob on the detection of anomalous bodies, and discuss the potential and apparent resistivity response characteristics of

the 3D complex borehole-to-surface model with vertical line source.

II. THEORY

In a homogeneous isotropic medium, the 3D boundary-value problem of a constant current point source underground is

$$
\begin{cases}
\nabla \cdot (\sigma \nabla \Phi) = -I\delta(P) \\
\sigma \dfrac{\partial \Phi}{\partial n} = 0 \quad \Gamma^s \\
\Phi = 0 \quad \Gamma^\infty
\end{cases}
\tag{1}
$$

where Φ is the electric potential (in units of V), σ the conductivity (in units of S/m), I the current intensity (in units of A), n the outer normal direction of the ground-air interface (Γ^s), and P the current source point. The inner boundary condition is a natural boundary condition and is not considered in the finite-element solution.

According to the variational principle, the variational problem corresponding to Eq. (1) is

$$
\begin{cases}
F(\Phi) = \dfrac{1}{2}\iiint \sigma\left[(\partial\Phi/\partial x)^2 + (\partial\Phi/\partial y)^2 + (\partial\Phi/\partial z)^2\right] \\
\qquad\qquad dV - \iiint I\delta(P)\Phi dV \\
\delta F(\Phi) = 0 \\
\Phi = 0\Gamma^\infty
\end{cases}
\tag{2}
$$

The potential generated by the finite-length line current source in a uniform underground medium can be regarded as a superposition of the potential generated by dividing the line source into n segments of small line sources, with each small line source acting as a point source. According to the superposition principle, we obtain the following potential variation problem under line source excitation when we integrate the first equation in Eq. (2) along the line source:

$$
\begin{cases}
F^*(\Phi) = \int \left\{ \dfrac{1}{2}\iiint \sigma[(\partial\Phi/\partial x)^2 + (\partial\Phi/\partial y)^2 \right. \\
\qquad\qquad \left. +(\partial\Phi/\partial z)^2]dV - \iiint I\delta(P)\Phi dV \right\} dl \\
\delta F^*(\Phi) = 0 \\
\Phi = 0\Gamma^\infty
\end{cases}
\tag{3}
$$

After analyzing and arranging the elements of Eq. (3), we obtain a large set of linear equations for solving any line source borehole-to-surface potential problem:

$$
Bx = f
\tag{4}
$$

where B is a large sparse coefficient matrix, x the node potential to be determined, and f the source item expression. By solving the linear equation set (4), the potential value of the node to be solved can be obtained.
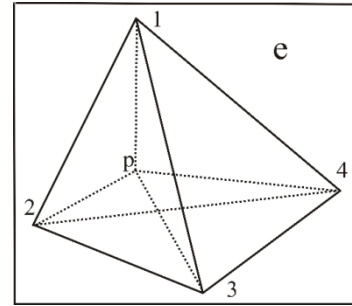

FIGURE 1. Tetragonal unit e.

To better deal with irregular multi-scale complex models, in this paper we use an adaptive segmentation model calculation zone with unstructured tetrahedral mesh (Figure 1). The potential at any point p(x, y, z) in unit e can be expressed by the calculated node potential and the interpolation function:

$$
\Phi_p = \sum N_i \Phi_i
\tag{5}
$$

where N_i and Φ_i are the interpolation value and potential, respectively, at node i in unit e.

The analytical expression of the potential of the borehole-to-surface model with a vertical line source in a half-space of isotropic and homogeneous medium is, (6) as shown at the bottom of this page, where ρ is the resistivity (in units of $\Omega\cdot$m) of the stratum; l_1, l_2, l_{1b}, and l_{2b} are, respectively, the top and bottom burial depths of the transmission and return line sources (in units of m); z_p is the depth of the measurement point (in units of m); and r_p and r_{bp} are, respectively, the radial distances (in units of m) of the measuring point from the transmission and return line sources. In the calculation in this paper, we take $l_1 = l_{1b}$ and $l_2 = l_{2b}$.

$$
\Phi = \frac{I\rho}{4\pi(l_2 - l_1)}\ln\frac{\left(l_2 - z_p + \sqrt{(l_2 - z_p)^2 + r_p^2}\right)\left(l_2 + z_p + \sqrt{(l_2 + z_p)^2 + r_p^2}\right)}{\left(l_1 - z_p + \sqrt{(l_1 - z_p)^2 + r_p^2}\right)\left(l_1 + z_p + \sqrt{(l_1 + z_p)^2 + r_p^2}\right)}
$$

$$
- \frac{I\rho}{4\pi(l_{2b} - l_{1b})}\ln\frac{\left(l_{2b} - z_p + \sqrt{(l_{2b} - z_p)^2 + r_{bp}^2}\right)\left(l_{2b} + z_p + \sqrt{(l_{2b} + z_p)^2 + r_{bp}^2}\right)}{\left(l_{1b} - z_p + \sqrt{(l_{1b} - z_p)^2 + r_{bp}^2}\right)\left(l_{1b} + z_p + \sqrt{(l_{1b} + z_p)^2 + r_{bp}^2}\right)}
\tag{6}
$$

In the numerical calculation of the borehole model, calculation errors may arise due to the presence of the steel casing, anomalous field source, boundary loading, and meshing partition. To minimize the influence of these factors on the calculation results to the greatest extent possible, we applied the data processing method for controllable marine electromagnetic data proposed by Kong *et al*. in 2008 to the borehole-to-surface electrical method [36]. We first find the total field potential and background field, that is, the field for homogeneous half-space, under the same mesh division, and then use their difference as the anomalous field potential. We then synthesize a new total field potential from the anomalous field potential and an analytical solution of the background field to improve the calculation accuracy. In the numerical calculation, the anomalous potential $\Phi_{difference}$ generated by the target body can be expressed by the total field potential Φ_{total} and background field potential $\Phi_{background}$. Here, the total field potential Φ_{total} and background field potential $\Phi_{background}$ of the model can both be obtained from Eq. (4). Therefore, the anomalous potential $\Phi_{difference}$ attributable to the target body only can be expressed as

$$\Phi_{difference} = \Phi_{total} - \Phi_{background} \qquad (7)$$

The total field potential can be expressed as

$$\Phi_{total} = \Phi_{background} + \Phi_{difference} \qquad (8)$$

In the anomalous potential obtained from Eq. (7), the common errors in the total field potential and background field potential caused by the boundary loading effect and field source processing have been eliminated. In the case of a homogeneous half-space or a layered model, the potential can be solved analytically, but the background field potential obtained by numerical calculation contains errors. Therefore, we replace the $\Phi_{background}$ in Eq. (8) with the analytical solution $\Phi_{analytic}$ to meet the higher accuracy requirement of the newly synthesized total field potential:

$$\Phi_{new\ total} = \Phi_{analytic} + \Phi_{difference} \qquad (9)$$

To obtain Φ_{total} and $\Phi_{background}$ from Eq. (4), the high accuracy level of the total field potential obtained from Eq. (9) can be assured without densely meshing the region in which the field sources are located. This reduces the order of the equation to be solved.
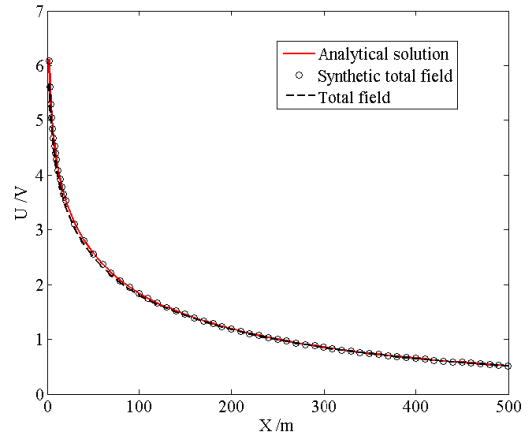

FIGURE 2. Comparison of numerical solution and analytic solution for homogeneous half-space.

By synthesizing a new total field potential, the following formula may be used to solve for the apparent resistivity of the borehole-to-surface electrical method:

$$\rho = \frac{\Delta\Phi}{I}\frac{1}{K_M - K_N} \qquad (10)$$

where $\Delta\Phi = \Phi_M - \Phi_N$, M and N are the measuring electrodes, I is the current intensity (in units of A), and the device coefficient K is, (11) as shown at the bottom of this page.

III. MODEL CALCULATION AND ANALYSIS

To verify the calculation accuracy, the homogeneous half-space model (100 $\Omega \cdot$ m) is viewed as a superposition of a homogeneous half-space background medium (95 $\Omega \cdot$ m) and a homogeneous half-space anomaly (5 $\Omega \cdot$ m). The length of the line source is 300 m, and the return line source is set at 4000 m from the transmission source (the same below), and the current intensity is 20 A (the same below). The analytic solution of the potential of the homogeneous half-space model (100 $\Omega \cdot$ m) is obtained from Eq. (6). The potential of the synthetic total field is obtained by the finite-element method described above, and the total field potential is obtained from Eq. (4). The numerical solution is compared with the analytic solution of the homogeneous half-space model (100 $\Omega \cdot$ m) and the results are shown in Fig. 2. The numerical solution and analytic solution basically overlap.

$$K = \frac{1}{4\pi\,(l_2 - l_1)}\left(\ln\frac{\left(l_2 - z_p + \sqrt{(l_2 - z_p)^2 + r_p^2}\right)\left(l_2 + z_p + \sqrt{(l_2 + z_p)^2 + r_p^2}\right)}{\left(l_1 - z_p + \sqrt{(l_1 - z_p)^2 + r_p^2}\right)\left(l_1 + z_p + \sqrt{(l_1 + z_p)^2 + r_p^2}\right)} \right.$$
$$\left. - \ln\frac{\left(l_2 - z_p + \sqrt{(l_2 - z_p)^2 + r_{bp}^2}\right)\left(l_2 + z_p + \sqrt{(l_2 + z_p)^2 + r_{bp}^2}\right)}{\left(l_1 - z_p + \sqrt{(l_1 - z_p)^2 + r_{bp}^2}\right)\left(l_1 + z_p + \sqrt{(l_1 + z_p)^2 + r_{bp}^2}\right)} \right) \qquad (11)$$

The test results demonstrated the reliability of the calculation accuracy of the new method proposed here for calculating the line source. In Fig. 2, the abscissa is the transmission and reception distance (in units of m) and the ordinate is the electric potential (in units of V).
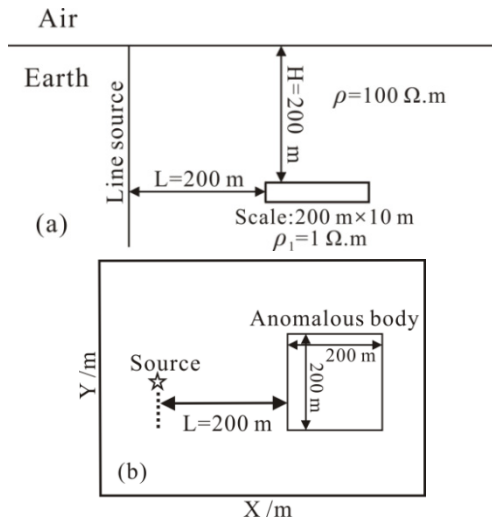

FIGURE 3. Schematics of (a) cross-sectional and (b) planar views of model.

A. MODEL 1: VALIDATION OF NEW ALGORITHM

To verify the processing effect of the new algorithm, a geo-electric model is designed, shown in Fig. 3, in which the length of the line source is 500 m, and a low-resistivity anomaly with a resistivity of $1 \ \Omega \cdot m$ and a size of 200 m $\times$ 200 m $\times$ 10 m (along the x, y, and z directions) is present in the homogeneous half-space with a background medium resistivity of $100 \ \Omega \cdot m$. The left-hand side of the buried anomaly is 200 m from the source and the top surface is at a depth of 200 m. Figure 4 shows the results of the planar apparent resistivity calculated from Eq. (4) [Fig. 4(a)] and the planar apparent resistivity calculated using Eq. (9) [Fig. 4(b)]. It can be seen that both Figs. 4(a) and 4(b) satisfactorily reflect the position and shape of the anomalous body (the white frame in the figure), but the method using the total field potential newly synthesized from the anomalous field potential and the analytic solution of the background field [Fig. 4(b)] can more effectively eliminate the calculation noise from the background.

B. MODEL 2: INFLUENCE OF LINE SOURCE LENGTH ON DETECTION USING BOREHOLE- TO-SURFACE METHOD

To study the effects of the length of line current source on the sensitivity for detecting anomalies with the borehole-to-surface method, we designed the 3D model shown in Fig. 5. In the model, only the length of the line source is changed and all other parameters remain the same. In the homogeneous half-space medium with a resistivity of $100 \ \Omega \cdot m$, a low-resistivity anomaly with a resistivity of $1 \ \Omega \cdot m$ and a size of 150 m $\times$ 150 m $\times$ 5 m (along the x, y, and z directions) is
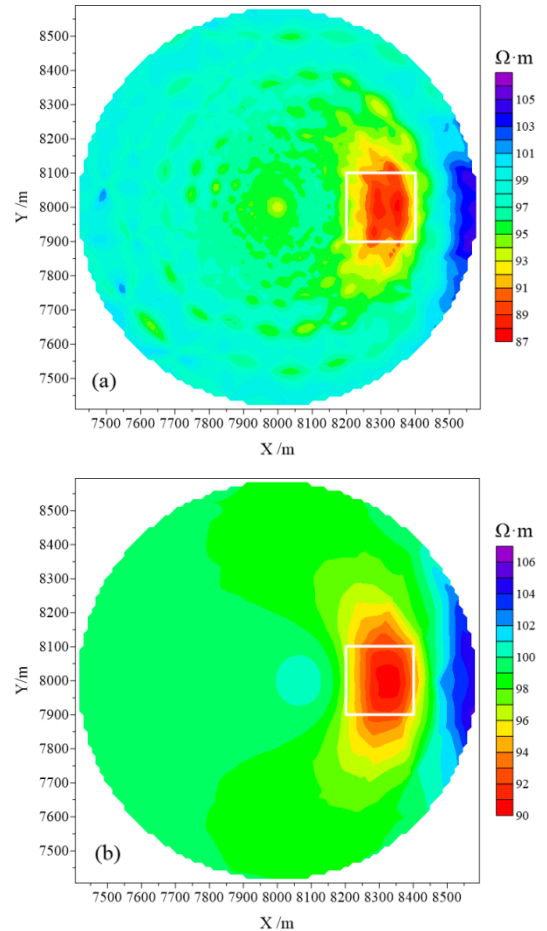

FIGURE 4. Apparent-resistivity contour map in planar view: Planar view apparent resistivity calculated from (a) Eq. (4) and (b) Eq. (9).
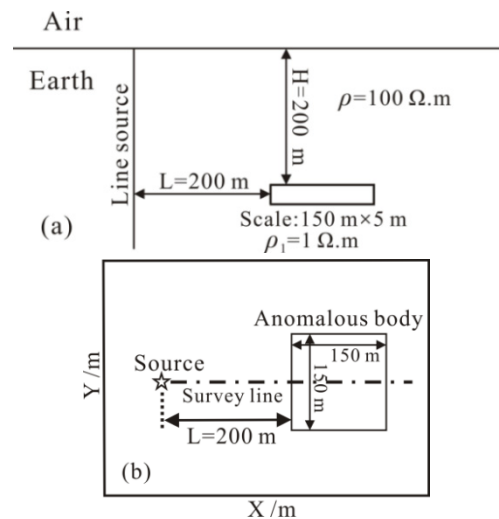

FIGURE 5. Schematics of (a) cross-sectional and (b) planar views fo the model.

buried at a distance of 200 m from the source and at a depth of 200 m to the top surface. With the transmitting borehole as the center, detection lines are arranged in a circular network. The apparent resistivity on the ground surface is calculated for the following respective lengths of the line current source:
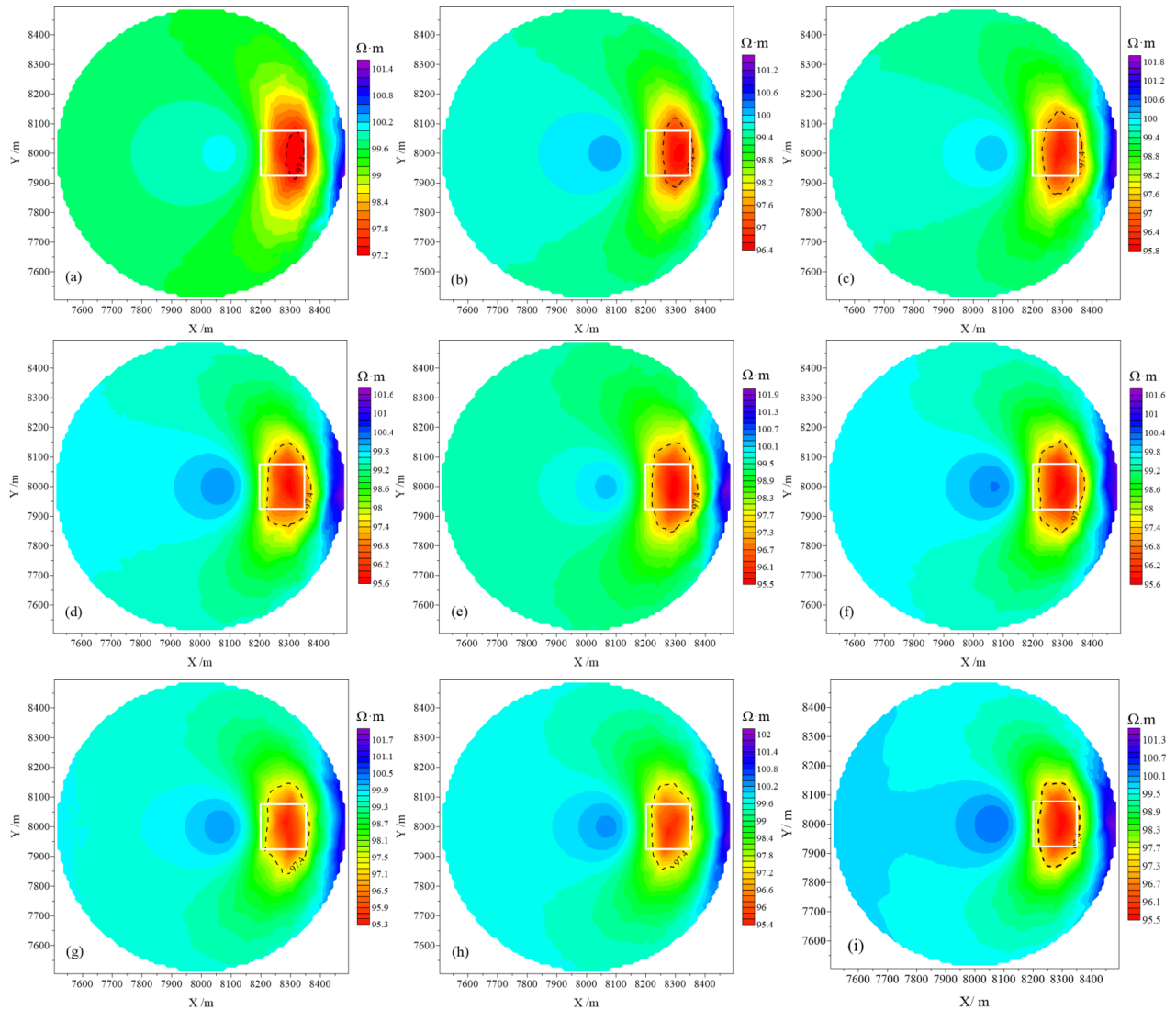
FIGURE 6. (a)–(i) Ground surface apparent-resistivity contour maps corresponding to line source lengths of 100 (a), 200 (b), 300 (c), 400 (d), 500 (e), 700 (f), 1000 (g), 1500 (h), and 2000 m (i).

100, 200, 300, 400, 500, 700, 1000, 1500, and 2000 m. Figures 5(a) and 5(b) are the schematic cross-sectional and plane views, respectively, of the model. Figures 6(a)–6(i) correspond, respectively, to the apparent surface resistivity contour (white frame in the figure indicates the boundary of the anomaly) for the following lengths of the line current source: 100, 200, 300, 400, 500, 700, 1000, 1500, and 2000 m. The horizontal and vertical coordinates represent the position of the measuring points (in units of m). Figure 7 shows the apparent resistivity for different lengths of the line current source on the same line of measurement. The position of the measurement line is indicated in Fig. 5(b) with a black dotted line, the abscissa is the transmission and reception distance (in units of m), and the ordinate is the apparent resistivity (in units of $\Omega \cdot$ m).

A comparison of the results in Figs. 6 and 7 shows that, as the length of the line source increases within a certain range, the detection efficiency of the borehole-to-surface
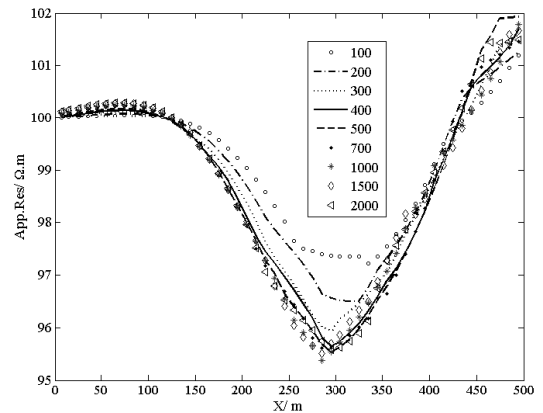

FIGURE 7. Apparent-resistivity curves for different lengths of line source along the same measurement line.

electrical method for the low-resistivity anomaly gradually improves. However, this does not imply that the longer the length of the transmission source, the better the
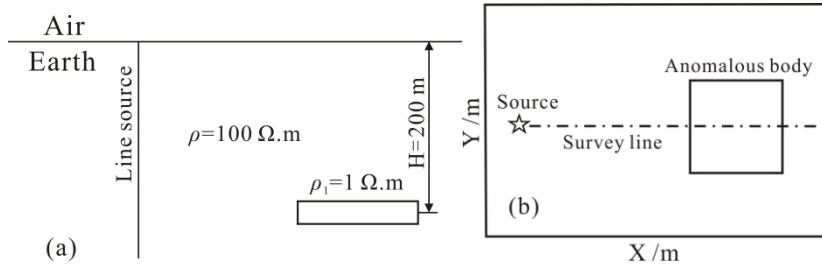
FIGURE 8. Schematics of (a) cross-sectional and (b) planar views of the model.

detection efficiency. When the length of the line source exceeds a certain value, continued increase of the line source length has little effect on the detection efficiency of the anomalies. In terms of the planar apparent resistivity, the size of the low-apparent-resistivity region at the low-resistivity anomaly has a tendency to increase as the length of the line source increases [as shown by the black dotted line in Figs. 6(a)–6(i)]. The apparent resistivity curves in Fig. 7 show that, as the length of line source increases, the minimum value of the apparent resistivity shows a tendency of moving from the side farther away from the source toward the center of the anomaly projected on the Earth's surface, but an excessively long line source is no longer sensitive to the detection of low-resistivity anomalies. The calculation results show that the optimum length of the excitation line source should be approximately 500 m. The efficiency of the borehole-to-surface method depends on the length of the line source relative to the burial depth of the anomaly. Within a certain range of the line source length and electric current intensity, more current flows through the low-resistivity anomaly as the length of line source increases, thereby improving the detection efficiency. However, when the length is excessive, it no longer improves the detection efficiency. Therefore, in the detection of targets with the borehole-to-surface method the excitation should be provided by a line source with a judiciously chosen length, and a longer source is not always better.

C. MODEL 3: SENSITIVITY OF BOREHOLE-TO-SURFACE METHOD IN DETECTING HORIZONTAL AND VERTICAL SCALES OF LOW-RESISTIVITY ANOMALY

To study the detection sensitivity of the borehole-to-surface method to changes of the horizontal and vertical scales of the low-resistivity anomaly, we designed the model shown in Fig. 8. The length of the line source is 500 m, and a low-resistivity anomaly with a resistivity of 1 $\Omega \cdot$ m is buried in a homogeneous half-space of 100 $\Omega \cdot$ m resistivity. The center of the anomaly is at a distance of 300 m from the transmitting source and at a depth of 200 m. The scales of the anomaly are set to 100 m × 100 m × 10 m, 100 m × 100 m × 40 m, and 200 m × 200 m × 10 m (along the x, y, and z directions), where the volume of the last two anomalies are equal. The position of the 600-m-long measurement line is shown as a black dotted line in Figure 8(b). Figure 8 shows schematic
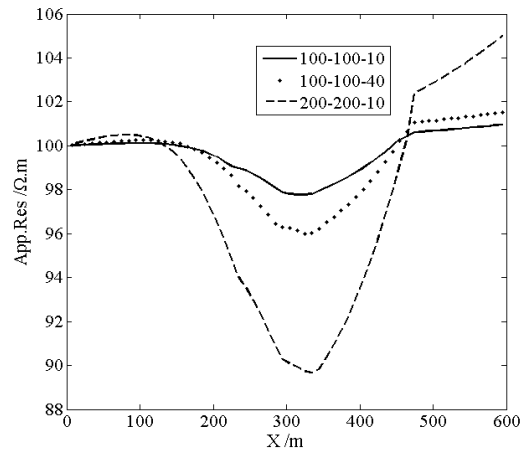

FIGURE 9. Comparison of apparent-resistivity curves for different scale parameters in horizontal and vertical directions.
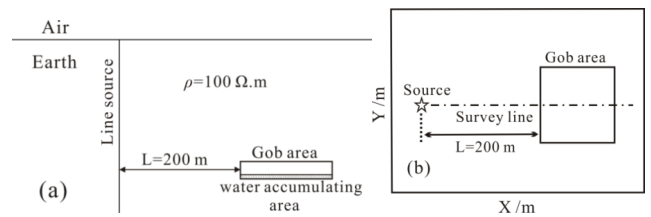

FIGURE 10. Schematics of (a) cross-section and (b) planar views of the model.

cross-sectional and planar views of the model and Figure 9 a comparison of the apparent resistivity curves for different size parameters in the horizontal and vertical directions. The abscissa is the transmission and reception distance (in units of m) and the ordinate is the apparent resistivity (in units of $\Omega \cdot$ m).

As can be seen from Fig. 9, the borehole-to-surface electrical method can clearly identify the presence of low-resistivity anomalies. As the size of the anomalous body increases, the detection efficiency of the borehole-to-surface method becomes more pronounced. For anomalies having the same volume, the detection efficiency is much more pronounced for anomalies with a large horizontal area or lateral spread (200 m × 200 m × 10 m), than for an anomaly with a large vertical thickness (100 m × 100 m × 40 m). Thus, the borehole-to-surface method is more sensitive to changes
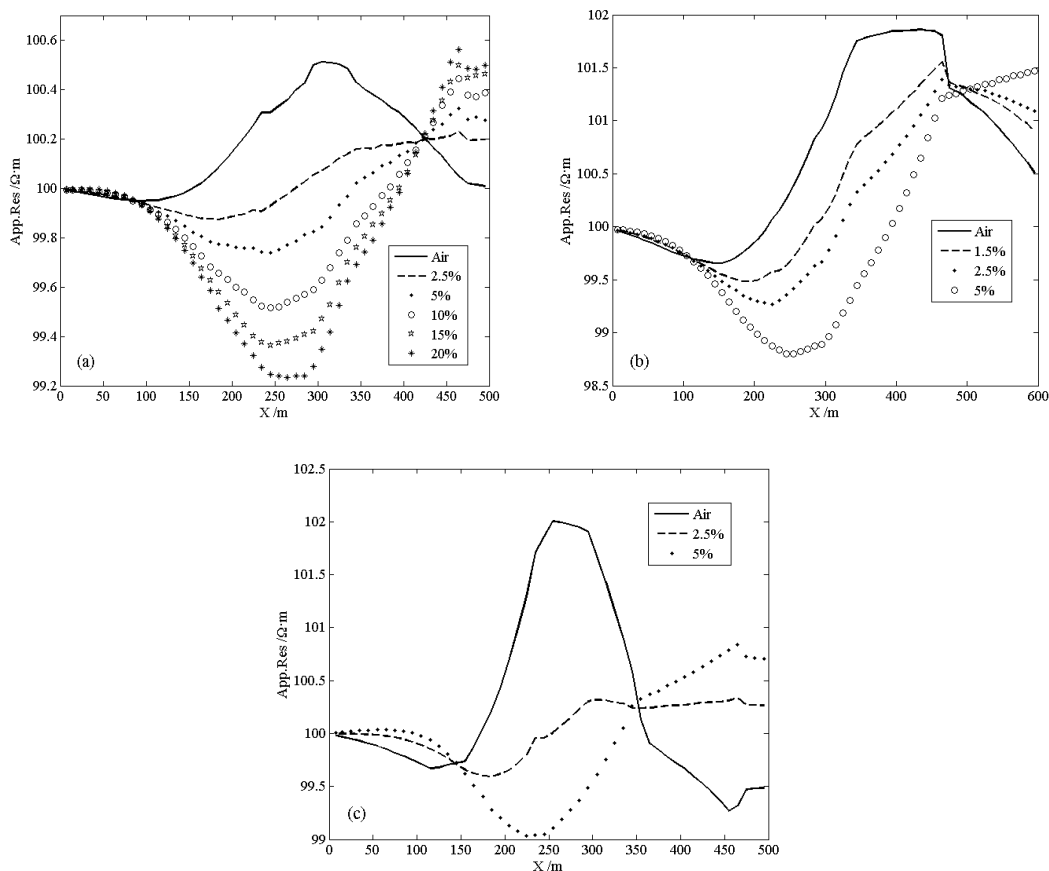
FIGURE 11. Apparent-resistivity curves for gobs buried at a depth of 200 m and having scales of (a) 100 m×100 m×20 m and (b) 200 m×200 m×20 m, and (c) for a gob buried at a depth of 100 m and having a scale of 100 m×100 m×20 m.

in the lateral area of the anomaly than to changes in its thickness.

D. MODEL 4: EFFECT OF VOLUME FRACTION OF WATER IN GOB ON DETECTION EFFICIENCY

To explore the factors that affect the detection efficiency of the borehole-to-surface method in a water-logged gob, we designed the model shown in Fig. 10. A homogeneous half-space of resistivity $100\ \Omega \cdot m$, contains a 20-m-thick gob. The length of the line current source is 500 m, the gob is located 200 m from the source, and the burial depth of the top surface is 200 m. The scales of the anomaly (along directions in the order of x, y, and z) are 200 m × 200 m × 20 m and 100 m × 100 m × 20 m, respectively. When the burial depth of the top surface is 100 m, the size of the gob is 100 m×100 m×20 m. By changing the volume fraction of water in the gob, we investigated the detection of the different water accumulation ratios in the gob. The resistivity of the accumulated water is taken to be $1\ \Omega \cdot m$ and the resistivity of the air layer is taken to be $10^9 \Omega \cdot m$. Figures 10(a) and 10(b), respectively, show the schematic cross-sectional and planar views of the model. Figures 11(a) and 11(b) show the apparent-resistivity curves for a 200-m gob for different water content ratios and 100 m × 100 m × 20 m and 200 m × 200 m × 20 m

anomalies, respectively. Figure 11(c) shows the apparent resistivity curve of a 100-m gob and a 100 m × 100 m × 20 m anomaly for different water content ratios. In Fig. 11, the abscissa is the transmission and reception distance (in units of m) and the ordinate is the apparent resistivity (in units of $\Omega \cdot m$). The position of the measurement line is shown as a black dotted line in Fig. 10(b).

Figure 11 shows that in the absence of water a gob as a whole exhibits high resistance. As the volume fraction of water increases in the gob, the apparent resistivity of the region in which anomalies distribute gradually decreases. When there is a small amount (e.g., 2.5%) of brine water in the gob, its apparent resistivity can already be distinguished from that of an air-filled gob, and begins to show a low-resistivity phenomenon. Therefore, the borehole-to-surface electrical method is more sensitive to low-resistivity anomalies, which is good for the detection of water-logged coal gobs, for preventing flooding accidents in mines, and for providing technical support for mining safety. The larger the volume fraction of water in the gob, the more obvious the decrease in resistivity, and the higher the accuracy of the location of the anomaly center, which is away from the transmitting side of the source. A comparison of the results in Figs. 11(a) and 11(b) shows that—for the same burial
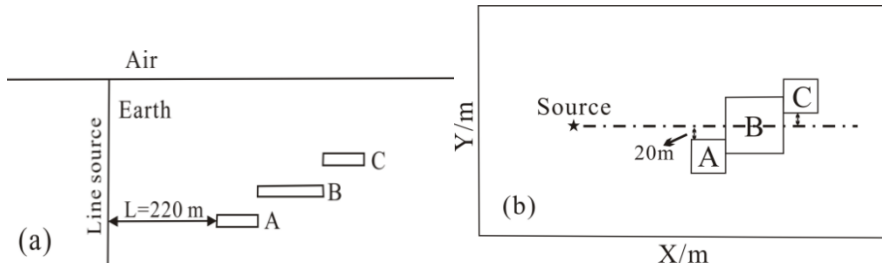
FIGURE 12. Schematics of (a) main cross-sectional and (b) planar views of the model.
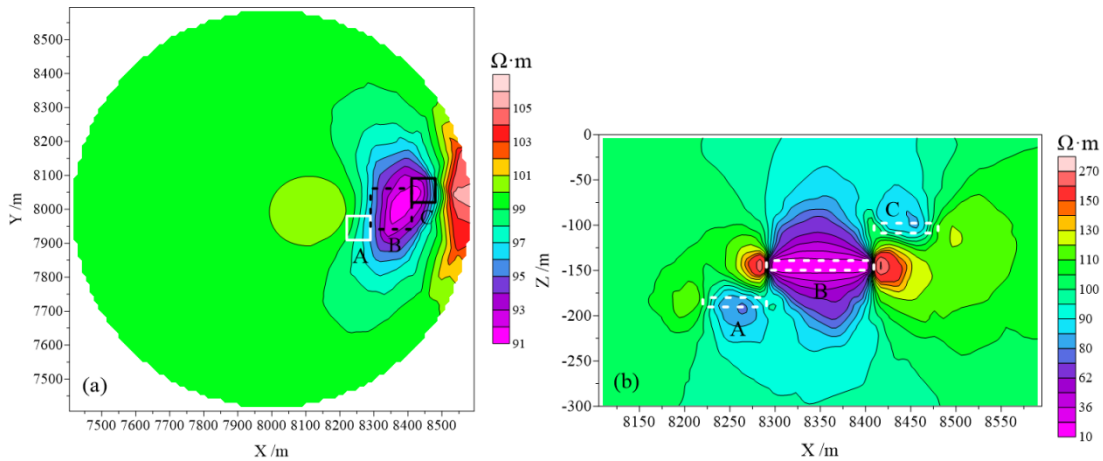

FIGURE 13. Apparent-resistivity contour maps for (a) planar and (b) main cross-sectional views.

depth and water content—the greater the extent of the gob, the easier it is for the borehole-to-surface method to detect water accumulated in the gob. For example, for a water volume fraction of 5%, the smaller anomaly of Fig. 11(a) shows a low resistivity of approximately 99.74 $\Omega \cdot$ m, but the larger anomaly of Fig. 11(b) shows a lower resistivity than that of Fig. 11(a), reaching a level of 98.7 $\Omega \cdot$ m. In addition, a comparison of Figs. 11(a) and 11(c) shows that a shallower buried depth is more favorable for the detection of a waterlogged gob. For the same volume fraction of water, the shallower the buried water-logged gob, the closer the resistivity value is to the true value. For example, for the same water content of 5%, the lowest apparent-resistivity value in Fig. 11(c) is approximately 99.03 $\Omega \cdot$ m. This example shows that the detection efficiency of a waterlogged gob depends not only on the volume fraction of water in the gob, but also on the depth and the size of the distributed area.

E. MODEL 5: RESULTS OF MULTI-ANOMALY COMPOUND MODEL

The model parameters are set as follows: The background resistivity of the homogeneous half-space is 100 $\Omega \cdot$ m, the length of the line source is 400 m, the sizes of the three low-resistivity anomalies (in order of A, B, and C and x, y, and z coordinates) are, respectively, 70 m $\times$ 70 m $\times$ 10 m, 120 m $\times$ 120 m $\times$ 10 m, and 70 m $\times$ 70 m $\times$ 10 m, and the top

surface burial depths are 180, 140, and 100 m, respectively. The resistivity of the anomaly is taken to be 1 $\Omega \cdot$ m. The horizontal distance between the left-hand side of the anomaly A and the source is 220 m, and the horizontal distance from the boundary of anomalies A and C to the main cross-sectional plane that goes through the source and center of anomaly B is 20 m. Figures 12(a) and 12(b) are schematics of the main cross-section and planar views, respectively, of the model. Figures 13(a) and 13(b) are contour maps of the apparent resistivity in the planar view and main cross-section, respectively, of the model (white or black frames in the figure are the boundaries of the anomaly), and the horizontal and vertical coordinates, in units of m, represent the coordinate position of the measurement point. The corresponding position of the main cross-section in the planar view is shown by the black dotted line in Fig. 12(b).

In the planar view of the apparent resistivity [Fig. 13(a)], anomalies A, B, and C are all visible to some extent, but the boundaries of anomaly A are not as clear as those of B and C since anomaly A, being closer to the source, is squeezed by the source current and is buried deeper than the others. In the cross-sectional view of the apparent resistivity profile [Fig. 13(b)], the presence of the three anomalies can be clearly identified. The main cross-section passes through the center of anomaly B, so the boundary of B is clearly defined. Anomaly B is revealed on the cross-sectional view with the

best accuracy because it is not only the largest anomaly, but the cross-section plane also happens to pass through the center of B. Since the two anomalies A and C are 20 m away from the main cross-section, their boundaries are not as clear as that of B, and their center positions are slightly offset downward and upward, respectively.

IV. CONCLUSION

Based on a finite-element method with unstructured mesh, we performed numerical calculations for the borehole-to-surface electrical potential method on a series of designed models. The calculations made use of the new method of the total field potential synthesized from the pure anomaly field and the analytic solution of the background field. This investigation led to the following important conclusions after studying the roles of the length of the line source, the vertical and horizontal size of the low-resistivity anomaly, the volume fraction of water in the gob, and the burial depth.

(1) The dependence of the detection efficiency on the length of the line source is related to the buried depth of the anomaly. For a given burial depth of the anomaly, the detection efficiency increases with increasing length of the line source within a certain range. However, when the line source is too long, it is of little significance for improving the detection of the anomaly.

(2) The borehole-to-surface electrical method is much more sensitive to changes in the horizontal scale of the low-resistivity anomaly than to changes in the vertical scale.

(3) A gob can exhibit the phenomenon of low resistivity anomaly by retaining only a small amount of brine water. The detection efficiency of the borehole-to-surface electrical method depends on the volume fraction of water in the gob, burial depth, and size of the gob.

(4) The borehole-to-surface electrical method can clearly define the boundary positions of the anomaly. The side of the anomaly closer to the source on the plane is susceptible to the effects of the source current, but the boundary of the anomaly can be more accurately delineated.

REFERENCES

[1] R. E. Nimmer and J. L. Osiensky, "Using mise-à-la-masse to delineate the migration of a conductive tracer in partially saturated basalt," *Environ. Geosci.*, vol. 9, no. 2, pp. 81–87, 2002, doi: 10.1046/j.1526-0984.2002.92005.x.

[2] S. R. Pant, "Tracing groundwater flow by mise-à-la-masse measurement of injected saltwater," *J. Environ. Eng. Geophys.*, vol. 9, no. 3, pp. 155–165, 2004, doi: 10.4133/jeeg9.3.155.

[3] P. David, T. V. Carlos, and Z. Y. Zhang, "Sensitivity study of borehole-to-surface and crosswell electromagnetic measurements acquired with energized steel casing to water displacement in hydrocarbon-bearing layers," *Geophysics*, vol. 73, no. 6, pp. F261–F268, 2008, doi: 10.1190/1.2993538.

[4] M. T. Perri, G. Cassiani, I. Gervasio, R. Deiana, and A. Binley, "A saline tracer test monitored via both surface and cross-borehole electrical resistivity tomography: Comparison of time-lapse results," *J. Appl. Geophysics*, vol. 79, pp. 6–16, Apr. 2012, doi: 10.1016/j.jappgeo.2011.12.011.

[5] Q. W. Dai, D. P. Chen, and H. F. Liu, "3D FEM modeling of the borehole-to-surface potential method with complex pipe network linear current source," (in Chinese), *Oil Geophys. Prospecting*, vol. 47, no. 6, pp. 998–1005, Dec. 2012.

[6] L. De Carlo, M. T. Perri, M. C. Caputo, R. Deiana, M. Vurro, and G. Cassiani, "Characterization of a dismissed landfill via electrical resistivity tomography and mise-à-la-masse method," *J. Appl. Geophys.*, vol. 98, pp. 1–10, Nov. 2013, doi: 10.1016/j.jappgeo.2013.07.010.

[7] K.-G. Zhu, Z.-S. Jia, Y.-Z. Wang, Z.-F. Li, C.-L. Qiu, T.-T. Li, X.-T. Li, and J. Lin, "Research on borehole-surface joint electrical double-parameter monitoring for the hydraulic fracturing in oilfields," (in Chinese), *Chin. J. Geophys.*, vol. 56, no. 11, pp. 3663–3672, Nov. 2013, doi: 10.6038/cjg20131107.

[8] D. Chen, Q. Dai, H. Liu, and D. Feng, "3-D forward modeling and analysis of borehole-surface potential with gradient source," (in Chinese), *J. Central South Univ. (Sci. Technol.)*, vol. 45, no. 1, pp. 150–156, Jan. 2014.

[9] P.-S. Zhang, J.-S. Wu, Y.-H. Zhao, and S.-A. Xu, "Testing simulation and application of the borehole-ground joint parallel electrical method," (in Chinese), *Geol. Explor.*, vol. 51, no. 5, pp. 964–969, Sep. 2015, doi: 10.13712/j.cnki.dzykt.2015.05.017.

[10] C.-W. Li, B.-Y. Ruan, Y.-Z. Lu, C.-S. Duan, T.-W. Yang, and J.-L. Wang, "Three-dimensional FEM modeling of point source borehole-ground electrical potential measurements," (in Chinese), *Chin. J. Geophys.*, vol. 53, no. 3, pp. 729–736, Mar. 2010, doi: 10.3969/j.issn.0001-5733.2010.03.028.

[11] M. Zhou, G. Lin, and H. Zhang, "Pt catalyst supported on multiwalled carbon nanotubes for hydrogenation-dearomatization of toluene," (in Chinese), *Chin. J. Catal.*, vol. 28, no. 3, pp. 210–216, Mar. 2007, doi: 10.1016/S1872-2067(07)60020-5.

[12] P. D. Zhao, S. T. Zhang, and J. P. Chen, "Discussion on prediction and appraisement of replaceable resources of crisis mine," (in Chinese), *J. Chengdu Univ. Technol. (Sci. Technol. Ed.)*, vol. 31, no. 2, pp. 111–117, Apr. 2004.

[13] Z. L. Huang, *Gravity Magnetism Electricity Method in Petroleum Prospecting*, 1st ed. Beijing, China: Petroleum Univ. Press, (in Chinese), 1999, pp. 347–355.

[14] L. Alfano, "Geoelectric prospecting with underground electrodes," *Geophys. Prospecting*, vol. 10, pp. 290–303, 1961, doi: 10.1111/j.1365-2478.1962.tb02015.x.

[15] D. F. Pridmore, G. W. Hohmann, S. H. Ward, and W. R. Sill, "An investigation of finite-element modeling for electrical and electromagnetic data in three dimensions," *Geophysics*, vol. 46, no. 7, pp. 1009–1024, 1981, doi: 10.1190/1.1441239.

[16] J. P. Rocroi and A. V. Koulikov, "The use of vertical line sources in electrical prospecting for hydrocarbon," *Geophys. Prospecting*, vol. 33, no. 1, pp. 138–152, 1985, doi: 10.1111/j.1365-2478.1985.tb00426.x.

[17] H. Scriba, "Computation of the electric potential in three-dimensional structures," *Geophys. Prospecting*, vol. 29, no. 5, pp. 790–802, 1981, doi: 10.1111/j.1365-2478.1981.tb00710.x.

[18] K. Spitzer, "A 3-D finite-difference algorithm for DC resistivity modelling using conjugate gradient methods," *Geophys. J. Int.*, vol. 123, no. 3, pp. 903–914, 1995, doi: 10.1111/j.1365-246X.1995.tb06897.x.

[19] K. Ushijima, H. Mizunaga, and T. Tanaka, "Reservoir monitoring by a 4-D electrical technique," *Lead. Edge*, vol. 18, no. 12, pp. 1422–1424, Dec. 1999, doi: 10.1190/1.1438242.

[20] J. H. Yue and Z. X. Liu, "Three dimension resistivity tomography of mine ground," (in Chinese), *Progr. Geophys.*, vol. 20, no. 2, pp. 104–109, Jun. 2005.

[21] Z.-G. Wang, Z.-X. He, W.-B. Wei, M. Deng, and Z.-G. Wang, "3-D physical model experiments of well-to-ground electrical survey," (in Chinese), *Oil Geophys. Prospecting*, vol. 40, no. 5, pp. 594–597, Oct. 2005, doi: 10.13810/j.cnki.issn.1000-7210.2005.05.020.

[22] K.-J. Xu, T.-L. Li, H. Zhang, J.-P. Li, "3D resistivity inversion of vertical finite line source using conjugate gradients," (in Chinese), *Coal Geol. Explor.*, vol. 34, no. 3, pp. 69–71, Jun. 2006.

[23] W. Zhigang, H. Zhanxiang, and W. Wenbo, "3D modeling and born approximation inversion for the borehole surface electromagnetic method," *Appl. Geophys.*, vol. 4, no. 2, pp. 84–88, Jul. 2007, doi: 10.1007/s11770-007-0012-0.

[24] Z.-G. Wang, Z.-X. He, W.-B. Wei, X.-J. Liu, B.-Y. Tang, and Z.-G. Wang, "3-D quasi-analytic approximate inversion of borehole-to-surface electric data," (in Chinese), *Oil Geophys. Prospecting*, vol. 42, no. 2, pp. 220–225, Apr. 2007, doi: 10.13810/j.cnki.issn.1000-7210.2007.02.021.

[25] J.-T. Tang, J.-F. Zhang, B. Feng, J.-Y. Lin, and C.-S. Liu, "Determination of borders for resistive oil and gas reservoirs by deviation rate using the hole-to-surface resistivity method," (in Chinese), *Chin. J. Geophys.*, vol. 50, no. 3, pp. 926–931, May 2007.

[26] Y.-H. Qu, G.-B. Zhang, L.-F. Zhao, and Z.-J. Wen, "Study on 3-D resistivity inversion for infinite surface-borehole line current source," (in Chinese), *Progr. Geophys.*, vol. 22, no. 5, pp. 1393–1402, Oct. 2007, doi: 10.3969/j.issn.1004-2903.2007.05.009.

[27] T. L. Ho, "3-D inversion of borehole-to-surface electrical data using a back-propagation neural network," *J. Appl. Geophysics*, vol. 68, no. 4, pp. 489–499, 2009, doi: 10.1016/j.jappgeo.2008.06.002.

[28] Q.-W. Dai, D.-P. Chen, H.-F. Liu, and D.-S. Feng, "Research of the residual oil dstribution with dual frequency induced polarization and the borehole-to-surface potential method," (in Chinese), *Prog. Geophys.*, vol. 24, no. 3, pp. 959–964, Jun. 2009, doi: 10.3969/j.issn.1004-2903.2009.03.018.

[29] G. Ke and Q. Huang, "3D forward and inversion problems of borehole-to-surface electrical method," (in Chinese), *Acta Sci. Naturalium Univ. Pekinensis*, vol. 45, no. 2, pp. 264–272, Mar. 2009, doi: 10.13209/j.0479-8023.2009.041.

[30] H. Cao, L. Mao, X. Wang, and K. Wang, "Physical simulation experiment on borehole-to surface electromagnetic responses," (in Chinese), *Oil Geophys. Prospecting*, vol. 48, no. 6, pp. 995–998, Dec. 2013, doi: 10.13810/j.cnki.issn.1000-7210.2013.06.021.

[31] Z. Wang and H. Pan, "Research on the enhanced algorithms of the abnormal response characteristics for 3D borehole-to-surface resistivity method," (in Chinese), *Geophys. Prospecting Petroleum*, vol. 53, no. 4, pp. 491–500, Jul. 2014, doi: 10.3969/j.issn.1000-1441.2014.04.016.

[32] Y.-Y. Zhang, D.-J. Liu, G.-X. Zhu, Q.-H. Ai, and M.-J. Qin, "3D forward modeling of borehole-to-surface electric potential measurement system," (in Chinese), *Prog. Geophys.*, vol. 30, no. 4, pp. 1849–1855, Aug. 2015, doi: 10.6038/pg20150445.

[33] Z. Wang, H.-P. Pan, Y.-H. Luo, S.-N. Fang, and H.-J. Fang, "3-D hole-to-surface resistivity inversion with nonlinear conjugate method under the constraint of inequality," (in Chinese), *Prog. Geophys.*, vol. 31, no. 1, pp. 0360–0370, Feb. 2016, doi: 10.6038/pg20160142.

[34] Z. Wang, A. P. Wu, and G. Li, "Forward modeling of borehole-ground induced polarization method under undulating topography," (in Chinese), *Geophys. Prospecting Petroleum*, vol. 57, no. 6, pp. 927–935, Nov. 2018, doi: 10.3969/j.issn.1000-1441.2018.06.015.

[35] H. Q. Tan, J. S. Shen, and C. Zhou, "Borehole-to-surface electrical imaging technique and its application to residual oil distribution analysis of the eighth section in GuDong oilfield," (in Chinese), *J. China Univ. Petroleum (Ed. Natural Sci.)*, vol. 28, no. 2, pp. 31–37, Apr. 2004.

[36] F. N. Kong, S. E. Johnstad, and H. Westerdahl, "A 2.5D finite-element-modeling difference method for marine CSEM modeling in stratified anisotropic media," *Geophysics*, vol. 73, no. 1, pp. F9–F19, 2008, doi: 10.1190/1.2819691.

XINGONG TANG was born in Pingdingshan, Henan, China, in 1968. He received the bachelor's degree in well logging, in 1992, the master's degree in geophysical prospecting and information technology from Jianghan Petroleum University, in 1999, and the Ph.D. degree in geophysics from Peking University, in 2006. He has served on the teaching and research work of the School of Geophysics and Petroleum Resources, Yangtze University, where he is currently a Professor and a Doctoral Supervisor. He has hosted or participated in more than 30 national and business research projects. More than 90 academic articles have been published in various academic journals and international conferences. He holds three national invention patents and one U.S. invention patent. He is a member of the Chinese Geophysics Society (CGS), European Association of Geoscientists and Engineers (EAGE), and Society of Exploration Geophysicists (SEG), and the advisor of the Yangtze University SEG Student chapter. He received the first prize of Scientific Progress from China Petroleum and Chemical Industry Association, one second prize of Hebei Science and Technology Progress, one special Teaching Achievement Award of Yangtze University, one Teaching Distinguished Contribution Award, and four school-level Teaching Quality Excellence Awards of Yangtze University.

WEIZHONG QIU was born in Changzhou, Jiangsu, in 1963. He received the master's degree in engineering and an Engineer from the Taiyuan University of Technology, in 2006. He has been engaged in the exploration of coalfield geology and electromagnetics for a long time.

CHUNYAN ZHAO was born in Yuncheng, Shanxi, in 1994. She received the M.Sc. degree in solid earth physics from Yangtze University, in 2019. Her direction of study is electromagnetic prospecting. After graduation, she has been engaged in geological exploration with Shanxi Province 131 Coal Field Geology Limited Company.

ZHITAO XIONG was born in Lichuan, Hubei, in 1988. He received the bachelor's degree in geophysics and the master's degree from Yangtze University, in 2013 and 2016, where he is currently pursuing the Ph.D. degree in geodetection and information technology, and he focus mainly on the research of the theory and application of the electromagnetic exploration.

LIANQUN ZHANG was born in Xinyang, Henan, China, in 1988. He received the master's degree in earth exploration and information technology from Yangtze University, in 2014. In July 2014, he joined the China Petroleum Exploration and Development Research Institute and was mainly responsible for the interpretation of seismic and gravity and magnetic data processing. His research interests include gravity and magnetic seismic exploration and joint inversion.

● ● ●